1-1-2015

The diffusive Lotka-Volterra predator-prey system with delay

K S. Al Noufaey
University of Taif, ksnan708@uowmail.edu.au

T R. Marchant
University of Wollongong, tim@uow.edu.au

M P. Edwards
University of Wollongong, maureen@uow.edu.au

The diffusive Lotka-Volterra predator-prey system with delay

Abstract

Semi-analytical solutions for the diffusive Lotka-Volterra predator-prey system with delay are considered in one and two-dimensional domains. The Galerkin method is applied, which approximates the spatial structure of both the predator and prey populations. This approach is used to obtain a lower-order, ordinary differential delay equation model for the system of governing delay partial differential equations. Steady-state and transient solutions and the region of parameter space, in which Hopf bifurcations occur, are all found. In some cases simple linear expressions are found as approximations, to describe steady-state solutions and the Hopf parameter regions. An asymptotic analysis for the periodic solution near the Hopf bifurcation point is performed for the one-dimensional domain. An excellent agreement is shown in comparisons between semi-analytical and numerical solutions of the governing equations.

Disciplines

Engineering | Science and Technology Studies

Publication Details

Al Noufaey, K. S., Marchant, T. R. & Edwards, M. P. (2015). The diffusive Lotka-Volterra predator-prey system with delay. Mathematical Biosciences, 270 30-40.

The diffusive Lotka-Volterra predator-prey system with delay

K.S. Al Noufaey[1], T. R. Marchant[2] and M. P. Edwards[2]

[1] Mathematics and Statistics Department,
Faculty of Science, University of Taif,
Taif, Saudi Arabia

[2] School of Mathematics and Applied Statistics
The University of Wollongong, Wollongong, 2522, N.S.W., Australia.
email: tim_ marchant@uow.edu.au

Abstract. Semi-analytical solutions for the diffusive Lotka-Volterra predator-prey system with delay are considered in one and two-dimensional domains. The Galerkin method is applied, which approximates the spatial structure of both the predator and prey populations. This approach is used to obtain a lower-order, ordinary differential delay equation model for the system of governing delay partial differential equations. Steady-state and transient solutions and the region of parameter space, in which Hopf bifurcations occur, are all found. In some cases simple linear expressions are found as approximations, to describe steady-state solutions and the Hopf parameter regions. An asymptotic analysis for the periodic solution near the Hopf bifurcation point is performed for the one-dimensional domain. An excellent agreement is shown in comparisons between semi-analytical and numerical solutions of the governing equations.

Keywords. reaction-diffusion equations, Lotka-Volterra predator-prey model, Hopf bifurcations, semi-analytical solutions.

1 Introduction

Population models, which are used in a variety of biological and ecological applications, have been studied extensively for many decades. It is often important that these models include both time-delay and spatial diffusion to reflect the dynamic behavior of the models, based on past history, and the trend of a species to migrate to the least densely populated areas. Delay reaction-diffusion models, which display oscillatory solutions, can describe the lagged response to past behaviour and the spatial structure of certain chemical, biological and ecological systems. Some examples include the delayed logistic diffusion equation which represents the general framework of the growth dynamics of a single species and the delayed diffusive Lotka-Volterra predator-prey systems for multiple population models [4, 9, 21].

Alfred Lotka and Vito Volterra [15] proposed a model for predator-prey systems to describe the population of sharks and fish in the Adriatic Sea during World War I. This model can also be used to describe chemical reactions and physical systems such as resonantly coupled lasers [11, 15]. Many theoretical and experimental studies have considered the stability of the Lotka-Volterra predator-prey model. For example, Faria [8] considered the system with one and two delays. They studied the effect of diffusion and obtained the stability of the positive equilibrium and the location of Hopf bifurcation points. Yan and Chu [22] analyzed the stability for a delayed Lotka-Volterra predator-prey system and found conditions for oscillatory solutions to occur. They also examined the stability of the oscillatory solutions.

Chen et al. [5] considered the diffusive Lotka-Volterra predator-prey system with two delays. By analyzing the characteristic equations, the authors investigated the stability of Hopf bifurcations and the coexistence equilibrium. They found that the positive equilibrium point of the system could be destabilized through a Hopf bifurcation as the delay increases in magnitude. Shenghu [20] studied the dynamics of the diffusive Lotka-Volterra predator-prey model with prey-stage structure. They showed the effect of large diffusion rates on the existence of the positive steady states. A large diffusion rate for the prey species can lead to the destruction of spatial patterns while a large diffusion rate for the predator species preserves spatial patterns. Galiano et al. [10] examined the Lotka-Volterra predator-prey model with

cross-diffusion terms numerically and analytically. The authors proved the existence of a global weak solution in any number of space dimensions. Also, the numerical results for the 1-D domain were shown, underlining the effects of segregation of the species. Zhang and Zhao [23] considered a delayed diffusive three species Lotka-Volterra system and analysed the Hopf bifurcations of the system. These also presented numerical solutions of stable and oscillatory solutions to illustrate the effects of both delay and diffusion.

Usually, a system of ordinary differential equations (ODEs) can be analyzed by standard techniques. However reaction-diffusion equations are also important in many physically relevant modelling scenarios and are not so easily analyzed. Marchant [16] considered semi-analytical solutions for the Gray & Scott cubic autocatalytic model in a reaction-diffusion cell. The governing partial differential equation (PDE) model was approximated by a lower-order ODE model, using the Galerkin method of averaging. The ODE model was analyzed using various techniques from combustion theory which allowed bifurcation diagrams and Hopf bifurcation parameter maps to be found. An excellent comparison between the results of the semi-analytical method and the numerical solutions of the governing PDEs was found. The Galerkin averaging method has been applied to various other problems including a class of generalized diffusive logistic delay equations [2], the reversible Selkov model with feedback delay [3] and extensions to the Gray-Scott model such as Michaelis-Menten decay [17].

Fagan et al. [7] explored the importance of habitat edge effects, or boundary conditions, on species interactions and illustrated a number of scenarios using diffusive Lokta-Volterra equations. They gave physical examples of the different types of boundary conditions and related them to mathematical definitions. Scenarios considered included edge induced changes to migration patterns and mortality, cross-boundary subsidies and new types of interactions.

In this paper, the Lotka-Volterra predator-prey model with two delays is examined in both 1-D and 2-D domains where the Galerkin method is used to develop semi-analytical solutions. In §2 governing equations are presented and the Galerkin method is used to obtain the delay differential equations (DDEs) which represent the semi-analytical model. In §3 the steady-state concentration profiles and response diagrams are presented and described in detail. In §4 a local stability analysis of the semi-analytical model is performed. The Hopf points are found and the parameter region in which Hopf bifurcations occur is identified. In §5 the periodic solution near the Hopf bifurcation is developed for the semi-analytical DDE model for the 1-D domain. Comparisons are made throughout the paper between the semi-analytical results and numerical solutions of the governing PDEs.

2 The semi-analytical model

2.1 The governing equations

The Lotka-Volterra predator-prey model with two delays is considered in 1-D and 2-D domains. The governing PDEs and boundary conditions in 2-D are

$$\begin{aligned} u_t &= D_1(u_{xx} + u_{yy}) + u(\alpha - \gamma_1 u - \delta_1 v(t-\tau_1)), \\ v_t &= D_2(v_{xx} + v_{yy}) + v(-\beta + \gamma_2 u(t-\tau_2) - \delta_2 v), \qquad (1) \\ u_x &= v_x = 0, \text{ at } x = 0, \ u_y = v_y = 0, \text{ at } y = 0, \ u = v = 0, \text{ at } x = y = 1, \\ u &= u_\phi, \text{ at } -\tau_2 < t \leq 0 \text{ and } v = v_\phi \text{ at } -\tau_1 < t \leq 0. \qquad (2) \end{aligned}$$

The system (1) is in non-dimensional form with the scaled concentrations of the prey population density, u, and the predator population density, v. The 1-D system is the natural simplification of (1), where there are no y-variations. The boundary conditions at $x = y = 0$ are zero-flux Neumann boundary conditions while at $x = y = 1$ fixed population, Dirichlet boundary conditions are applied. Hence, it is an open system which allows the existence of steady-state solutions and sustained periodic oscillations. At $x = y = 0$ the zero-flux boundary conditions can either be interpreted as an impermeable boundary, which the species cannot cross or a simple symmetry condition. Fagan et al. [7] refers to this type of boundary condition as a "fence effect" and gives an example of the edges between old growth forests and clear-cuts as a boundary red-backed voles will not cross. As a fixed zero population boundary condition

is applied at $x = y = 1$ the region beyond can be interpreted as lethal to the species. Fagan et al. [7] gives examples of the applicability of Dirchelet boundary conditions such as Bison crossing national park boundaries (outside of which they are shot) and beetles crossing into cleared land (where they die of dessication).

The system has ten other parameters; α and β represent the growth rate of the prey species and the death rate of the predator species, respectively. The parameters γ_1 and δ_2 are the carrying capacity of the prey u and the predator v populations. δ_1 is the decrease in the population of the prey due to the predator presence, while γ_2 denotes the growth in the population of predator, due to the existence of the prey. The parameters τ_1 and τ_2 represent the hunting and predator maturation delays. The parameters D_1 and D_2 are the diffusion coefficients of the two species u and v. Note that all parameters are positive for physically realistic population models.

Numerical solutions of (1) and (2) are found using a Crank-Nicholson finite-difference scheme with accuracy of $O(\Delta t, \Delta x^2)$, while a fourth-order Runge-Kutta method is used to solve the DDE models.

2.2 The Galerkin method

The Galerkin method is used to obtain the semi-analytical model for the Lotka-Volterra predator-prey model (1) in 1-D and 2-D domains. This method assumes a spatial structure of the population density profiles, allowing the governing PDEs (1) and boundary conditions (2) to be approximated by a set of lower-order ODEs. The expansion

$$\begin{aligned} u(x,t) &= u_1(t)\cos\left(\frac{1}{2}\pi x\right) + u_2(t)\cos\left(\frac{3}{2}\pi x\right), \\ v(x,t) &= v_1(t)\cos\left(\frac{1}{2}\pi x\right) + v_2(t)\cos\left(\frac{3}{2}\pi x\right), \end{aligned} \tag{3}$$

is used which represents a two-term method in the 1-D spatial domain. Expansion (3) satisfies the boundary conditions (2), but not the governing PDEs. The form of basis functions (3) also has the property that the concentrations at the impermeable boundary $x = 0$ are $u = u_1 + u_2$ and $v = v_1 + v_2$. The free parameters in (3) are found by evaluating averaged versions of the governing equations, weighted by the basis functions. This process gives the following DDEs

$$\begin{aligned} \frac{du_1}{dt} &= -\frac{\pi^2 D_1 u_1}{4} - \frac{8\gamma_1 u_1^2}{3\pi} - \frac{16\gamma_1 u_1 u_2}{15\pi} + \alpha u_1 - \frac{8\delta_1 u_1 v_{1d}}{3\pi} - \frac{8\delta_1 u_1 v_{2d}}{15\pi} \\ &- \frac{8\delta_1 u_2 v_{1d}}{15\pi} - \frac{72\delta_1 u_2 v_{2d}}{35\pi} - \frac{72\gamma_1 u_2^2}{35\pi}, \\ \frac{dv_1}{dt} &= -\frac{\pi^2 D_2 v_1}{4} - \frac{8\delta_2 v_1^2}{3\pi} - \frac{16\delta_2 v_1 v_2}{15\pi} - \beta v_1 + \frac{8\gamma_2 v_1 u_{1d}}{3\pi} + \frac{8\gamma_2 v_1 u_{2d}}{15\pi} \\ &+ \frac{8\gamma_2 v_2 u_{1d}}{15\pi} + \frac{72\gamma_2 v_2 u_{2d}}{35\pi} - \frac{72\delta_2 v_2^2}{35\pi}, \\ \frac{du_2}{dt} &= -\frac{9\pi^2 D_1 u_2}{4} - \frac{8\gamma_1 u_1^2}{15\pi} - \frac{144\gamma_1 u_1 u_2}{35\pi} + \alpha u_2 - \frac{8\delta_1 u_1 v_{1d}}{15\pi} + \frac{8\gamma_1 u_2^2}{9\pi} \\ &- \frac{72\delta_1 u_2 v_{1d}}{35\pi} - \frac{72\delta_1 u_1 v_{2d}}{35\pi} + \frac{8\delta_1 u_2 v_{2d}}{9\pi}, \\ \frac{dv_2}{dt} &= -\frac{9\pi^2 D_2 v_2}{4} + \frac{8\delta_2 v_2^2}{9\pi} - \frac{144\delta_2 v_1 v_2}{35\pi} - \beta v_2 + \frac{72\gamma_2 v_2 u_{1d}}{35\pi} - \frac{8\delta_2 v_1^2}{15\pi} \\ &+ \frac{8\gamma_2 v_1 u_{1d}}{15\pi} + \frac{72\gamma_2 v_1 u_{2d}}{35\pi} - \frac{8\gamma_2 v_2 u_{2d}}{9\pi}, \end{aligned} \tag{4}$$

where $u_{id} = u_i(t - \tau_2)$ and $v_{id} = v_i(t - \tau_1)$, $i = 1, 2$. The DDEs (4) are obtained by truncating the series (3) after two terms. It is found that a two-term method produces superior accuracy without excessive expression swell. The one-term solution (when $u_2 = v_2 = 0$) is also calculated for comparison purposes. The accuracy of the one and two-term series solutions can be estimated using Richardson extrapolation, see Nelson et al. [19] for an example of error

estimation for a reaction-diffusion equation governing self-heating in compost piles. For the 2-D spatial domain, the expansion

$$\begin{aligned} u(x,y,t) &= u_1(t)\cos\left(\frac{1}{2}\pi x\right)\cos\left(\frac{1}{2}\pi y\right) + u_2(t)\cos\left(\frac{3}{2}\pi x\right)\cos\left(\frac{1}{2}\pi y\right) \\ &+ u_2(t)\cos\left(\frac{1}{2}\pi x\right)\cos\left(\frac{3}{2}\pi y\right), \\ v(x,y,t) &= v_1(t)\cos\left(\frac{1}{2}\pi x\right)\cos\left(\frac{1}{2}\pi y\right) + v_2(t)\cos\left(\frac{3}{2}\pi x\right)\cos\left(\frac{1}{2}\pi y\right) \\ &+ v_2(t)\cos\left(\frac{1}{2}\pi x\right)\cos\left(\frac{3}{2}\pi y\right), \end{aligned} \tag{5}$$

represent the two-term method which is used here. Note that two terms in each series have the same coefficient (for the u series, the coefficient u_2 appears twice). This is because the solution is symmetric along the line $y = x$. The expansion (5) also satisfies the boundary condition (2). The following DDE model, for the 2-D spatial domain,

$$\begin{aligned} \frac{du_1}{dt} &= -\frac{\pi^2 D_1 u_1}{2} - \frac{64\gamma_1 u_1^2}{9\pi^2} - \frac{256\gamma_1 u_1 u_2}{45\pi^2} + \alpha u_1 - \frac{64\delta_1 u_1 v_{1d}}{9\pi^2} - \frac{128\delta_1 u_1 v_{2d}}{45\pi^2} \\ &- \frac{128\delta_1 u_2 v_{1d}}{45\pi^2} - \frac{18176\delta_1 u_2 v_{2d}}{1575\pi^2} - \frac{18176\gamma_1 u_2^2}{1575\pi^2}, \\ \frac{dv_1}{dt} &= -\frac{\pi^2 D_2 v_1}{2} - \frac{64\delta_2 v_1^2}{9\pi^2} - \frac{256\delta_2 v_1 v_2}{45\pi^2} - \beta v_1 + \frac{64\gamma_2 v_1 u_{1d}}{9\pi^2} + \frac{128\gamma_2 v_1 u_{2d}}{45\pi^2} \\ &+ \frac{128\gamma_2 v_2 u_{1d}}{45\pi^2} + \frac{18175\gamma_2 v_2 u_{2d}}{1575\pi^2} - \frac{18176\delta_2 v_2^2}{1575\pi^2}, \\ \frac{du_2}{dt} &= -\frac{5\pi^2 D_1 u_2}{2} - \frac{64\gamma_1 u_1^2}{45\pi^2} - \frac{18176\gamma_1 u_1 u_2}{1575\pi^2} + \alpha u_2 - \frac{64\delta_1 u_1 v_{1d}}{45\pi^2} - \frac{4352\gamma_1 u_2^2}{4725\pi^2} \\ &- \frac{9088\delta_1 u_2 v_{1d}}{1575\pi^2} - \frac{9088\delta_1 u_1 v_{2d}}{1575\pi^2} - \frac{4352\delta_1 u_2 v_{2d}}{4725\pi^2}, \\ \frac{dv_2}{dt} &= -\frac{5\pi^2 D_2 v_2}{2} - \frac{4352\delta_2 v_2^2}{4725\pi^2} - \frac{18176\delta_2 v_1 v_2}{1575\pi^2} - \beta v_2 + \frac{9088\gamma_2 v_2 u_{1d}}{1575\pi^2} - \frac{64\delta_2 v_1^2}{45\pi^2} \\ &+ \frac{64\gamma_2 v_1 u_{1d}}{45\pi^2} + \frac{9088\gamma_2 v_1 u_{2d}}{1575\pi} + \frac{4352\gamma_2 v_2 u_{2d}}{4725\pi^2}, \end{aligned} \tag{6}$$

is obtained by weighting the equations by the basis functions and averaging.

3 Steady-state solutions

The steady-state of both (4) and (6) (where the time derivative terms are all zero) represents a set of four transcendental equations ($f_i = 0, i = 1, .., 4$), which are solved numerically using Maple. For the one term case, $u_2 = v_2 = 0$, so in this case two transcendental equations are obtained.

Figures 1(a) and 1(b) show steady-state population density profiles u and v versus x, for the 1-D spatial domain. The parameters are $\alpha = 0.4$, $\gamma_1 = 0.1$, $D_1 = D_2 = 0.05$, $\delta_1 = 0.2$, $\gamma_2 = 0.7$, $\delta_2 = 0.5$, $\beta = 0.4$ and $\tau_1 = \tau_2 = 0$. The one and two-term semi-analytical and numerical solutions of (1) and (2) are shown. The prey and predator densities are both highest in the centre of the domain as movement of both species occurs across the domain boundaries, to maintain the fixed population densities of zero there. The one-term solutions have a density of $(u, v) = (1.51, 0.876)$ at $x = 0$. The two-term density peaks are $(u, v) = (1.44, 0.926)$ at $x = 0$, while the numerical densities are $(u, v) = (1.45, 0.922)$. It can be seen that the two-term expression produces an excellent approximation when compared with the numerical solution of the governing PDEs (1) and (2). The errors are less than 1% for the u and v population density. For the one-term approximation, the errors are slightly larger, but no greater than about 5%. The two-term solutions are superior to the one-term profile as they model flat u and v population density profiles more accurately.

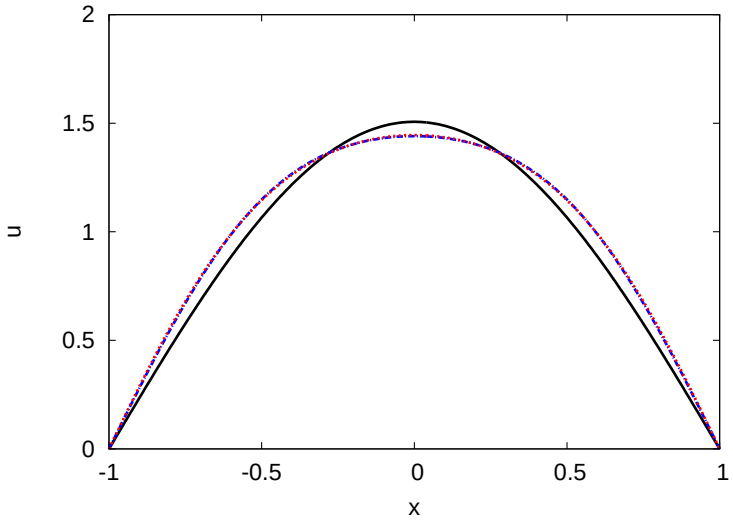

(a)

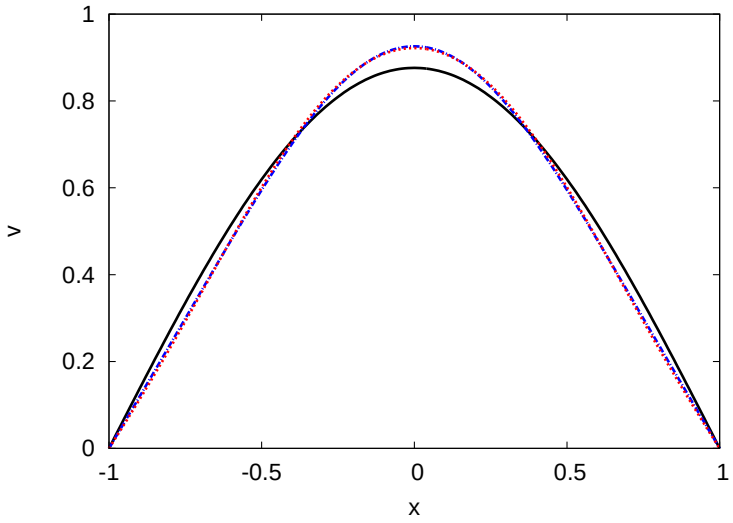

(b)

Figure 1: Steady-state prey, u (a), and predator, v (b), population density profiles versus x for the 1-D spatial domain. The parameters are $\alpha = 0.4$, $\gamma_1 = 0.1$, $D_1 = D_2 = 0.05$, $\delta_1 = 0.2$, $\gamma_2 = 0.7$, $\delta_2 = 0.5$, $\beta = 0.4$ and $\tau_1 = \tau_2 = 0$. The one-term (black solid line), two-term (blue dashed line) semi-analytical solutions and the numerical solution of (1) and (2) (red dotted line) are shown.

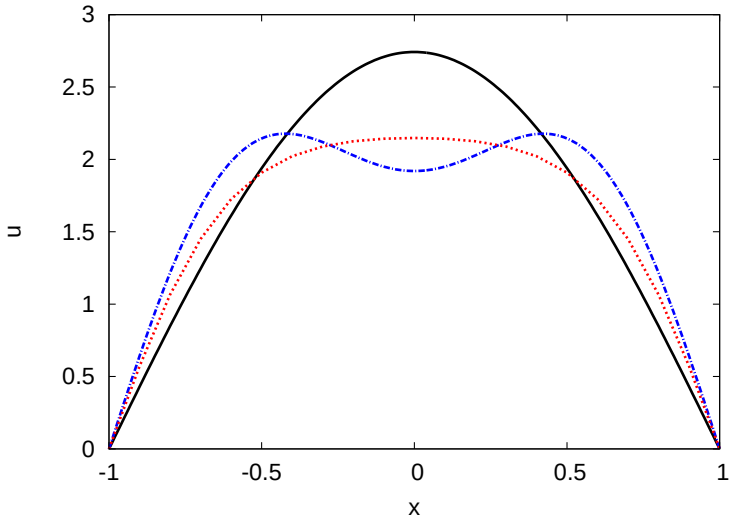

(a)

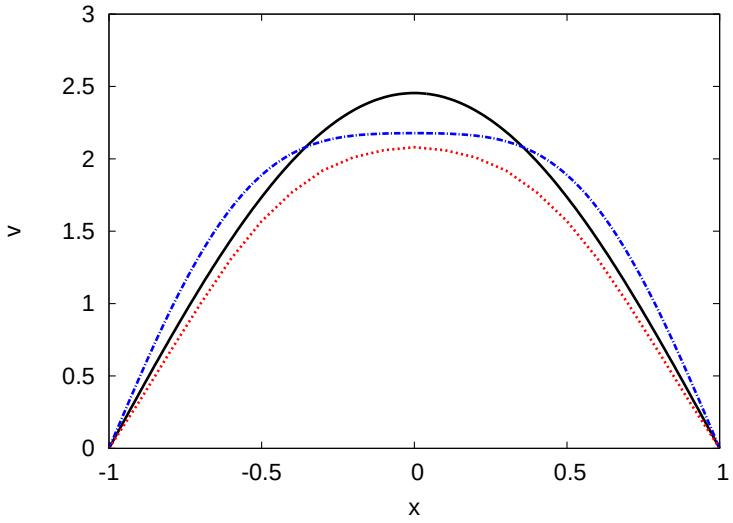

(b)

Figure 2: Steady-state prey, u (a), and predator, v (b), population density profiles versus x for the 2-D spatial domain. The parameters are $\alpha = 0.65$, $\gamma_1 = 0.1$, $D_1 = D_2 = 0.02$, $\delta_1 = 0.2$, $\gamma_2 = 0.7$, $\delta_2 = 0.5$, $\beta = 0.4$ and $\tau_1 = \tau_2 = 0$. The one-term (black solid line), two-term (blue dashed line) semi-analytical solutions and the numerical solution of (1) and (2) (red dotted line) are shown.

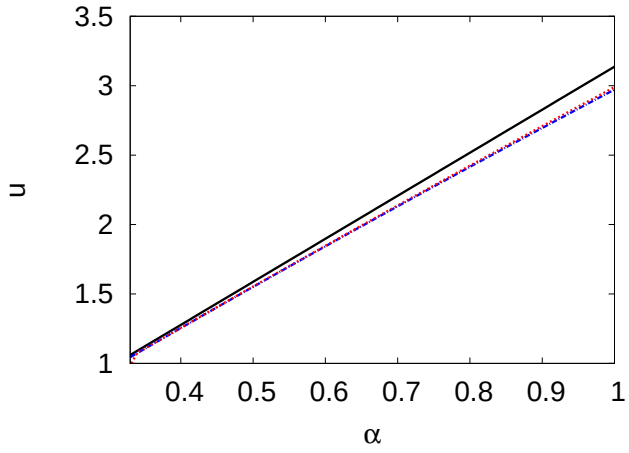

(a)

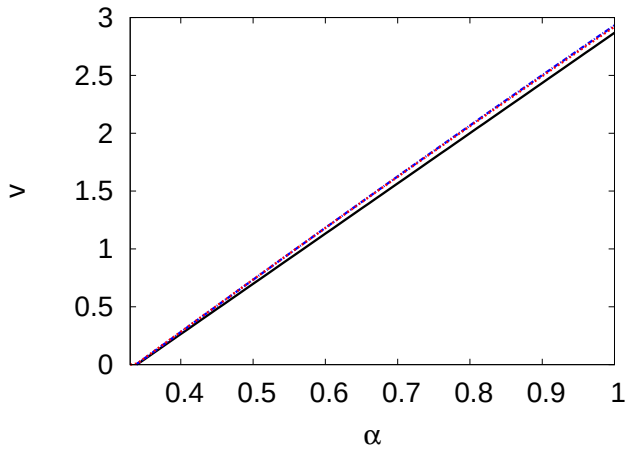

(b)

Figure 3: Steady-state population densities, u (a), and v (b), versus α for the 1-D spatial domain. The population densities are shown at $x = 0$. The parameters are $\gamma_1 = 0.1$, $D_1 = D_2 = 0.1$, $\delta_1 = 0.2$, $\gamma_2 = 0.7$, $\delta_2 = 0.5$, $\beta = 0.4$ and $\tau_1 = \tau_2 = 0$. The one-term (black solid line), two-term (blue dashed line) semi-analytical solutions and the numerical solution of (1) and (2) (red dotted line) are shown.

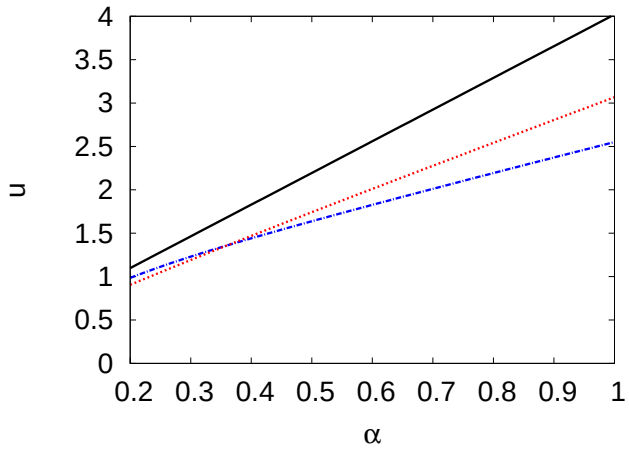

(a)

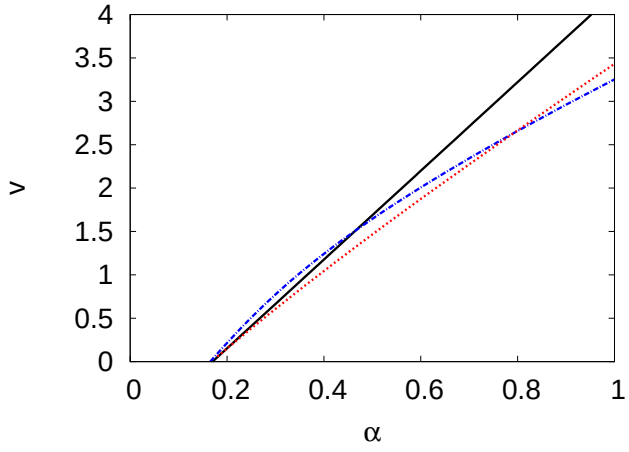

(b)

Figure 4: Steady-state population densities, u (a), and v (b), versus α for the 2-D spatial domain . The population densities are shown at $x = y = 0$. The parameters are $\gamma_1 = 0.1$, $D_1 = D_2 = 0.02$, $\delta_1 = 0.2$, $\gamma_2 = 0.7$, $\delta_2 = 0.5$, $\beta = 0.4$ and $\tau_1 = \tau_2 = 0$. The one-term (black solid line), two-term (blue dashed line) semi-analytical solutions and the numerical solution of (1) and (2) (red dotted line) are shown.

Figures 2(a) and 2(b) show steady-state population profiles u and v versus x, for the 2-D spatial domain respectively. The parameters are $\alpha = 0.65$, $\gamma_1 = 0.1$, $D_1 = D_2 = 0.02$, $\delta_1 = 0.2$, $\gamma_2 = 0.7$, $\delta_2 = 0.5$, $\beta = 0.4$ and $\tau_1 = \tau_2 = 0$. The one and two-term semi-analytical and numerical solutions of (1) and (2) are shown. The figures also show the profile through the centre of the domain, at $y = 0$. Moreover, at $x = 0$ the one and two-term solutions have densities of $(u, v) = (2.74, 2.46)$ and $(u, v) = (1.92, 2.18)$ respectively, while the numerical density is $(u, v) = (2.15, 2.08)$. For the one-term model, the errors are quite large at 28% and 18% for the u and v population density respectively. The two-term model gives a better comparison with the numerical solution. The errors are less than 11% and 5% for the u and v population densities. The numerical prey population density is very flat in the center of the domain and series solutions have difficult in modelling such profiles, hence the oscillatory two term profile. More series terms are needed to model flat profiles better.

Figures 3(a) and 3(b) show steady-state population densities u and v versus the bifurcation parameter α, for the 1-D spatial domain. The population densities are shown at $x = 0$. The parameters are $\gamma_1 = 0.1$, $D_1 = D_2 = 0.1$, $\delta_1 = 0.2$, $\gamma_2 = 0.7$, $\delta_2 = 0.5$, $\beta = 0.4$, $\tau_1 = \tau_2 = 0$. The steady state population densities increase in a near linear manner as α increases. The steady state two-term solutions can be approximated by $u = 2.92\alpha + 0.090$ and $v = 4.49\alpha - 1.51$. The solution v becomes positive at $\alpha = 0.34$ hence physically realistic solutions only exist for $\alpha \geq 0.34$. The two-term solution is very close to the numerical solution of the PDEs. At $\alpha = 1$ the numerical solutions are $(u, v) = (2.99, 2.92)$ while the one and two-term semi-analytical solutions are $(u, v) = (3.14, 2.87)$ and $(u, v) = (2.95, 2.89)$ respectively. The errors between the numerical and two-term semi-analytical solutions less than 2% for both the u and v population densities. While the one-term errors are no greater than about 5%.

Figures 4(a) and 4(b) show steady-state population densities u and v versus α, for the 2-D spatial domain respectively. The population densities are shown at $x = y = 0$. The parameters are $\gamma_1 = 0.1$, $D_1 = D_2 = 0.02$, $\delta_1 = 0.2$, $\gamma_2 = 0.7$, $\delta_2 = 0.5$, $\beta = 0.4$, $\tau_1 = \tau_2 = 0$. The one and two-term semi-analytical solutions and numerical solutions of the governing PDEs are shown. Again there is a near linear relationship between u, v and α. The one-term steady-state solution can be described by $u = 3.65\alpha + 0.368$, $v = 5.11\alpha - 0.869$. Here, the solution v is physically realistic solutions for $\alpha \geq 0.17$. At $\alpha = 0.6$, the errors between numerical and two-term semi-analytical solutions l are about 9% and 7%, for the u and v population density respectively.

4 Local stability, bifurcation diagrams and oscillatory solutions

A Hopf bifurcation occurs when oscillatory solutions exist in the neighborhood of a steady state whose stability is lost because of the crossing of a pair of complex conjugate eigenvalues over the imaginary axis. The Hopf bifurcation theory is explained in standard texts on bifurcation theory and dynamical systems [6, 12]. Here the stability of the semi-analytical model is analyzed and used to explore the effects of the two delays in altering the stability of the system (1) and (2), for both 1-D and 2-D spatial domains. The Hopf degeneracy points are calculated to find a semi-analytical map in which Hopf bifurcations occur and this prediction is compared with numerical results. Also bifurcation diagrams are drawn with two-term semi-analytical and numerical solutions compared. The bifurcations diagrams exhibit the steady-state amplitude solution branch and the maximum and minimum amplitudes of the oscillatory solutions. The amplitudes at $x = 0$, for the 1-D spatial domain, and at $x = y = 0$ for the 2-D spatial domain are shown.

The Hopf points are obtained by expanding in a Taylor series about the steady-state solution,

$$u_i(t) = u_{is} + \epsilon g_i e^{-\lambda t},\ v_i(t) = v_{is} + \epsilon h_i e^{-\lambda t},\ i = 1, 2. \tag{7}$$

We substitute (7) into the DDEs (4) (1-D domain) and (6) (2-D domain) and linearize around the steady state. The eigenvalues of the Jacobian matrix characterizes the perturbation in the system and we obtain a characteristic equation for λ. We set $\lambda = i\omega$ in the characteristic

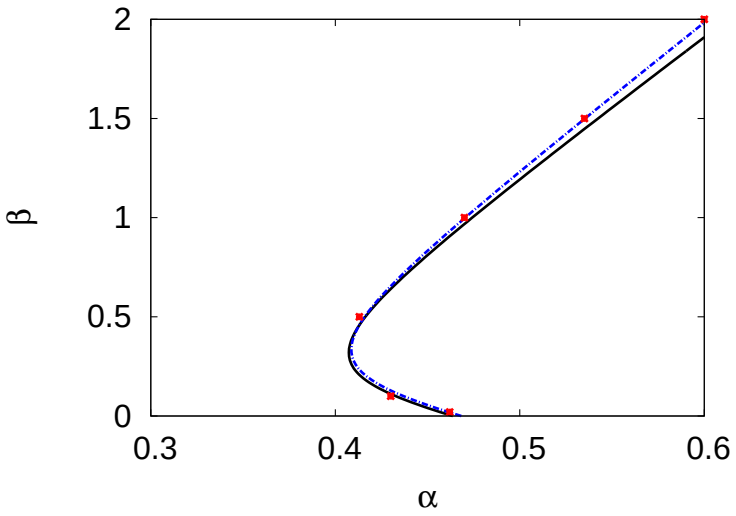

Figure 5: The regions of the α-β plane in which Hopf bifurcation can occur for the 1-D spatial domain. The one-term (black solid line), the two-term (blue, dashes) regions and the numerical solution (red, squares) are shown. The other parameters are $\gamma_1 = 0.1$, $D_1 = D_2 = 0.1$, $\delta_1 = 0.2$, $\gamma_2 = 0.7$, $\delta_2 = 0.5$ and $\tau_1 = \tau_2 = 4$.

equation and separate the real q_1 and imaginary q_2 parts. The Hopf bifurcation points occur at points where λ is purely imaginary, for more details see [18]. Here, the Hopf bifurcation points are found by solving the following conditions

$$f_1 = f_2 = f_3 = f_4 = q_1 = q_2 = 0. \tag{8}$$

Figure 5 shows the region in the α-β plane in which Hopf bifurcation occur for the 1-D spatial domain. Shown are the one and two-term semi-analytical solutions plus numerical solutions. The other parameters are $\gamma_1 = 0.1$, $D_1 = D_2 = 0.1$, $\delta_1 = 0.2$, $\gamma_2 = 0.7$, $\delta_2 = 0.5$ and $\tau_1 = \tau_2 = 4$. The semi-analytical solutions are found by solving (8). The Hopf curves break the plane into two regions. To the right of the curves Hopf bifurcation points occur while to the left only stable solutions occur. Generally speaking, a higher growth rate α destabilizes the system while a higher death rate β stabilizes it. The curve has a turning point at $(\alpha, \beta) = (0.410, 0.334)$ so Hopf bifurcations can only occur for $\alpha \geq 0.410$. The comparisons between the semi-analytical estimates and the numerical solutions, of the PDE model, are excellent. For example, at $\alpha = 0.6$, the numerical value at which Hopf bifurcations can occur is $\beta = 2$ while the one and two-term semi-analytical values are $\beta = 1.91$ and 1.98 respectively, which represents the errors of 5% and 2%.

Figure 6 shows the region in the α-β plane in which Hopf bifurcation occur for the 2-D spatial domain. Shown are the one and two-term semi-analytical solutions plus the numerical solution. The other parameters are the same as figure 5. Again to the right of the Hopf curves Hopf bifurcation points occur while to the left only stable solutions occur. Here, the turning point here is $(\alpha, \beta) = (0.657, 0.106)$ so Hopf bifurcations only occur for $\alpha \geq 0.657$. The errors are less than 5% and 2% for the one and two-term analytical solutions.

Figure 7 shows the regions in the τ_1-τ_2 plane in which Hopf bifurcation occur for the 1-D spatial domain. Shown are the one and two-term semi-analytical solutions and the numerical solution. The other parameters are $\alpha = 0.8$, $\beta = 0.4$, $\gamma_1 = 0.1$, $D_1 = D_2 = 0.1$, $\delta_1 = 0.2$,

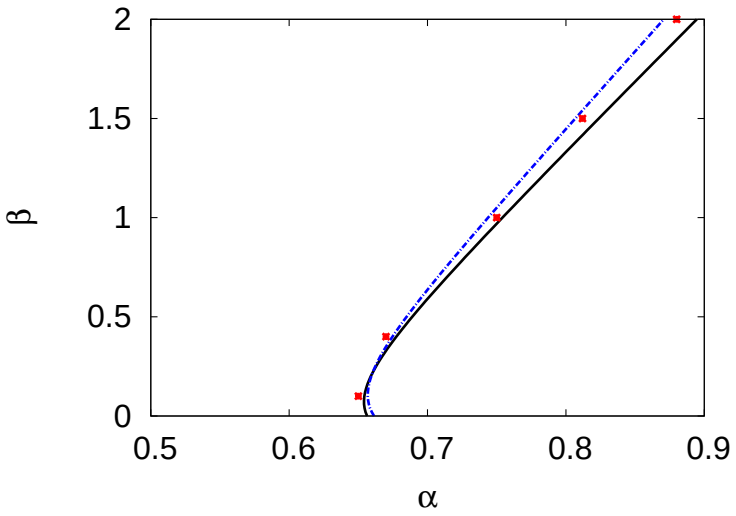

Figure 6: The regions of the α-β plane in which Hopf bifurcation can occur for the 2-D spatial domain. The one-term (black solid line), the two-term (blue, dashes) regions and the numerical solution (red, squares) are shown. The other parameters are $\gamma_1 = 0.1$, $D_1 = D_2 = 0.1$, $\delta_1 = 0.2$, $\gamma_2 = 0.7$, $\delta_2 = 0.5$ and $\tau_1 = \tau_2 = 4$.

$\gamma_2 = 0.7$ and $\delta_2 = 0.5$. The curves divide the plane into upper and lower regions. Above these curves limit cycles can occur while under the curves only stable solutions occur and there are no Hopf bifurcation points. In general, small values of the delay parameters leads to a stable solution while large delays, which implies feedback from the distant past, leads to instabilities [1, 2]. The Hopf curve of Hopf bifurcations can be described by the linear equations $\tau_2 = -0.994\tau_1 + 3.11$ and $\tau_2 = -\tau_1 + 3.23$ for one and two-term semi-analytical solutions respectively. Given the computational difficulty in obtaining estimates for arbitrary choices of the delay parameters, the linear equation approximations represent a simple and useful method for predicting the occurrence of Hopf bifurcations for this PDE system. At $\tau_1 = 1.60$, the one and two-term semi-analytical values are $\tau_2 = 1.51$ and $\tau_2 = 1.63$ while the numerical value is $\tau_2 = 1.60$. The errors are less than 6% and 2% respectively.

Figure 8 shows the regions in the τ_1-τ_2 plane in which Hopf bifurcation occur for the 2-D spatial domain. Shown are the one and two-term solutions and the numerical solution. The other parameters are the same as figure 5. The curves divide the plane into upper and lower regions. Above these curves limit cycles can occur while under the curves only stable solutions occur and there are no Hopf bifurcation points. The curve of Hopf bifurcations can be described by $\tau_2 = -\tau_1 + 4.28$ and $\tau_2 = -\tau_1 + 4.52$ for one and two-term semi-analytical solutions respectively. At $\tau_1 = 2.20$, the one and two-term semi-analytical values are $\tau_2 = 2.08$ and 2.32 while the numerical value is $\tau_2 = 2.20$. The errors in these estimates are less than 6%.

Figure 9(a) shows a limit cycle solution in the u versus v phase plane for $x = 0$, 0.33 and 0.66, while (b) and (c) show the evolution of u versus t, at $x = 0$ and 0.66 respectively, for the 1-D spatial domain. The parameters are $\alpha = 0.8$, $\beta = 0.4$, $\gamma_1 = 0.1$, $D_1 = D_2 = 0.1$, $\delta_1 = 0.2$, $\gamma_2 = 0.7$, $\delta_2 = 0.5$ and $\tau_1 = \tau_2 = 2$. Shown are the one and two-term semi-analytical and numerical solutions. The parameters lie above the Hopf curve in figure 7 so a limit cycle is possible. The figure illustrates the variations in the oscillatory solution as the

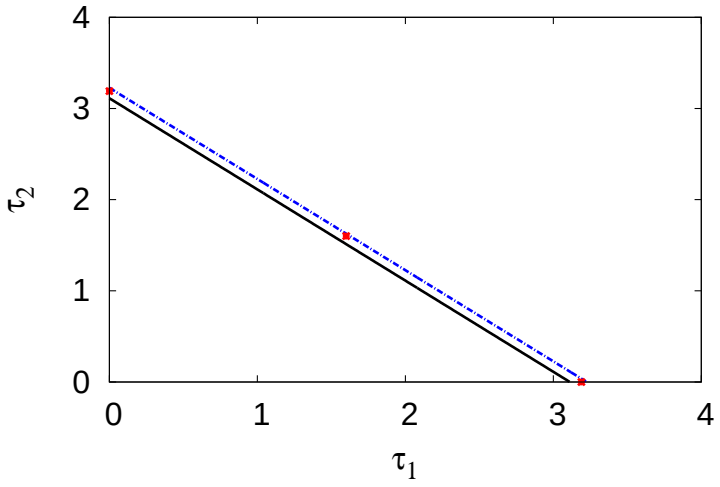

Figure 7: The regions of the τ_1-τ_2 plane in which Hopf bifurcation can occur for the 1-D spatial domain. The one-term (black solid line), the two-term (blue, dashes) regions and the numerical solution (red, squares) are shown. The other parameters are $\alpha = 0.8$, $\beta = 0.4$, $\gamma_1 = 0.1$, $D_1 = D_2 = 0.1$, $\delta_1 = 0.2$, $\gamma_2 = 0.7$ and $\delta_2 = 0.5$.

predator and prey populations are not uniform but vary through the domain. (3) represents the assumed spatial structure for the semi-analytical model. The period of the limit cycle is constant throughout the domain but the populations vary from a maximum at $x = 0$ to zero at the $x = 1$ boundary. The numerical period of the limit cycle is 1.72, while the one and two-term semi-analytical periods are 1.77 and 1.73. At $x = 0$ the limit cycle amplitudes are $(u, v) = (4.74, 5.85)$ (numerical), $(u, v) = (5.13, 6.09)$ (one-term) and $(u, v) = (4.76, 5.88)$ (two-term). At $x = 0$ the errors in the one and two-term semi-analytical values, are less than 8% and 1%. At intermediate locations in the domain the two-term semi-analytical solution is also very accurate. For $x = 0.33$ the comparisons are $(u, v) = (4.26, 5.03)$ (numerical) and $(u, v) = (4.30, 5.08)$ (two-term) while for $x = 0.66$ $(u, v) = (2.77, 2.98)$ (numerical) and $(u, v) = (2.80, 3.01)$ (two-term). Also, the time evolution curves for $x = 0$ and $x = 0.66$ show that the locations of the peaks and troughs do not depend on the location in the domain. Moreover the locations of the first few peaks, as predicted by the two-term semi-analytical solution, are very close to the corresponding numerical values.

Figure 10 shows the evolution of u versus t, for (a) $x = 0$, (b) $x = 0.33$ and (c) $x = 0.66$, for the 1-D domain. The parameters are $\alpha = 0.8$, $\beta = 0.4$, $\gamma_1 = 0.1$, $D_1 = D_2 = 0.1$, $\delta_1 = 0.2$, $\gamma_2 = 0.7$, $\delta_2 = 0.5$ and $\tau_1 = \tau_2 = 1$. Shown are one and two-term semi-analytical and numerical solutions. These parameters lie under the curve of figure 7 so a stable solution occurs. The figures shows that the transient behaviour is qualitatively similar at all locations in the domain, with the amplitude of the population oscillations decreasing as the $x = 1$ boundary is approached. When the time becomes large, the solution evolves to a steady-state. At $x = 0$ this steady-state solution is given by $(u, v) \simeq (2.52, 2.00)$ (one-term), $(u, v) \simeq (2.42, 2.07)$ (two-term) and $(u, v) \simeq (2.42, 2.07)$ (numerical). It can be seen that the two-term semi-analytical solution gives a good approximation, when compared with the numerical solution of the governing PDEs, of the steady-state values and of the relaxation oscillations, with only a 1% error for both population densities.

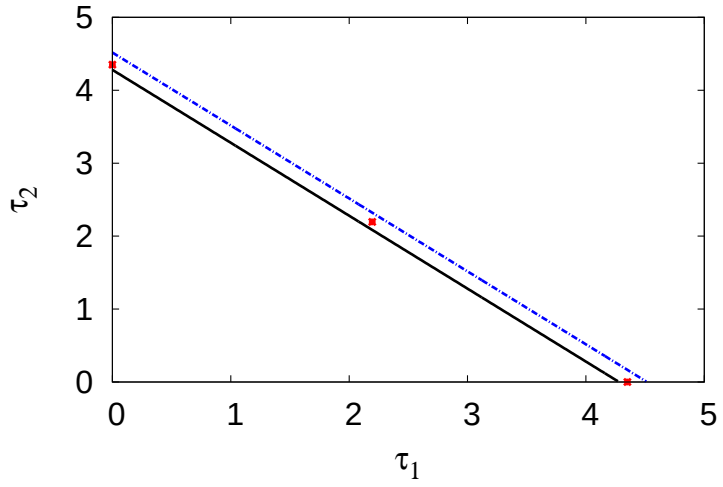

Figure 8: The regions of the τ_1-τ_2 plane in which Hopf bifurcation can occur for the 2-D spatial domain. The one-term (black solid line), the two-term (blue, dashes) regions and the numerical solution (red, squares) are shown. The other parameters are $\alpha = 0.8$, $\beta = 0.4$, $\gamma_1 = 0.1$, $D_1 = D_2 = 0.1$, $\delta_1 = 0.2$, $\gamma_2 = 0.7$ and $\delta_2 = 0.5$.

Figures 11(a) and (b) shows the bifurcation diagrams of population densities u and v, versus α , at $x = 0$, for the 1-D spatial domain. The parameters are $\beta = 0.4$, $\gamma_1 = 0.1$, $D_1 = D_2 = 0.1$, $\delta_1 = 0.2$, $\gamma_2 = 0.7$, $\delta_2 = 0.5$ and $\tau_1 = \tau_2 = 4$. Shown are the one and two-term semi-analytical and numerical solutions. The Hopf bifurcation point occurs at $\alpha = 0.410$ for both the one and two-term semi-analytical models, while the numerical value is $\alpha = 0.413$. The stable solution branch occurs for α less than the Hopf point value while the periodic solutions occur for larger α. Also, the values of v are non-negative for $\alpha \geq 0.34$ so physically realistic steady-state solutions occur for $\alpha \in [0.34, 0.41]$. The maximum amplitudes of the oscillations increases as α increases, while the minimum amplitudes of the oscillations become very small. It can be seen that the two-term semi-analytical solution gives an excellent approximation, when compared with the numerical solution of the governing PDEs, for both the stable and oscillatory solutions of the bifurcation diagram. The error in the one-term semi-analytical is no greater than 4%, while the two-term solution is the same as the numerical solution, to graphical accuracy.

Figures 12(a) and 12(b) show the bifurcation diagrams of population densities u and v, versus α , at $x = y = 0$, in the 2-D spatial domain. The parameter values are the same as figure 11. The one and two-term semi-analytical and numerical solutions are shown. For both one and two-term semi-analytical models the Hopf bifurcation point occurs at $\alpha = 0.679$ and $\alpha = 0.678$ respectively, while the numerical value is $\alpha = 0.677$. The errors for the 2-D domain are slightly larger than those for the 1-D case but are less than 15%.

Figure 13 shows the limit cycle curve u versus v at $x = 0$ for $\alpha = 1$ (inner curves), $\alpha = 1.25$ (middle curves) and $\alpha = 1.5$ (outer curves), for the 1-D domain. Shown is the two-term semi-analytical and numerical solutions. The parameters are $\beta = 0.4$, $\gamma_1 = 0.1$, $D_1 = D_2 = 0.1$, $\delta_1 = 0.2$, $\gamma_2 = 0.7$, $\delta_2 = 0.5$ and $\tau_1 = \tau_2 = 2$. This figure illustrates the nature of the limit cycle for larger α, well beyond the Hopf bifurcation point. Many biological systems, such as the Nicholsons blowflies equation (see, for example, Alfifi et al. [1]) exhibit

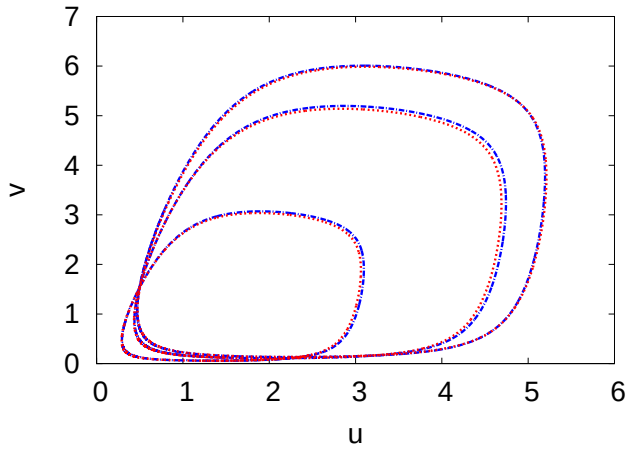

(a)

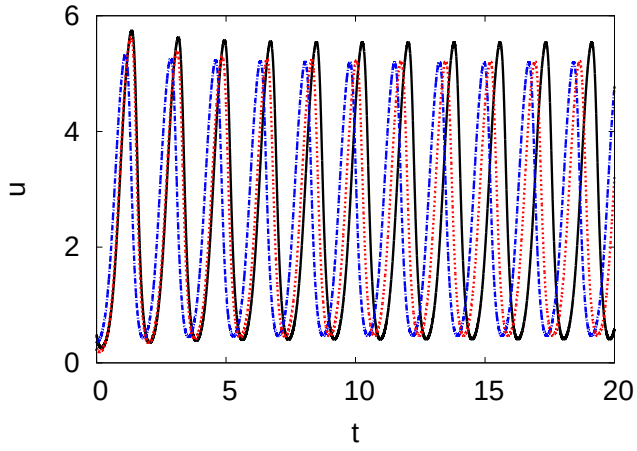

(b)

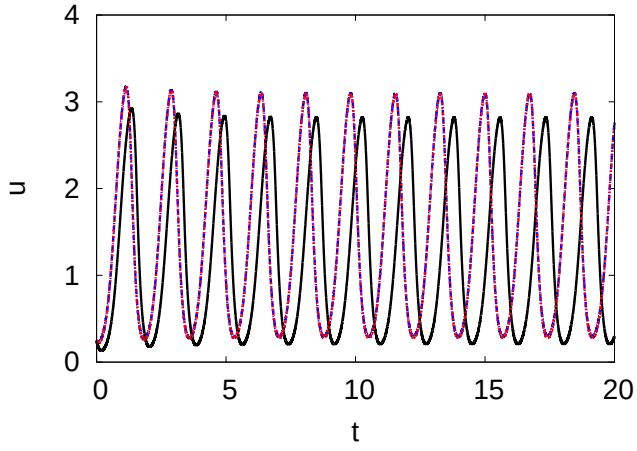

(c)

Figure 9: (a) The limit cycle curve u versus v, for $x = 0$ (outer curves) , $x = 0.33$ (middle curves) and $x = 0.66$ (inner curves) and the evolution of u versus t for (b) $x = 0$ and (c) $x = 0.66$, for the 1-D domain. Shown is the one-term semi-analytical solution (black, solid line), two-term semi-analytical solution (blue, dashed lines) and the numerical solution (red, dotted lines). The parameters are $\alpha = 0.8$, $\beta = 0.4$, $\gamma_1 = 0.1$, $D_1 = D_2 = 0.1$, $\delta_1 = 0.2$, $\gamma_2 = 0.7$, $\delta_2 = 0.5$ and $\tau_1 = \tau_2 = 2$.

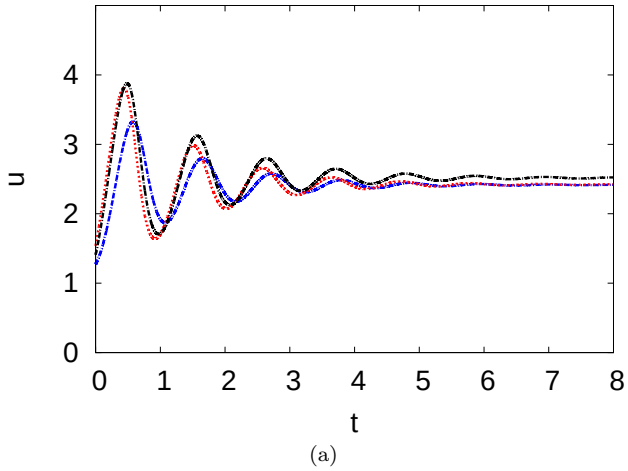

(a)

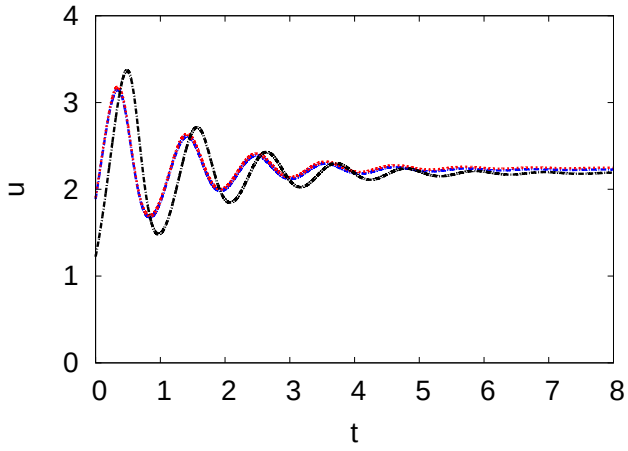

(b)

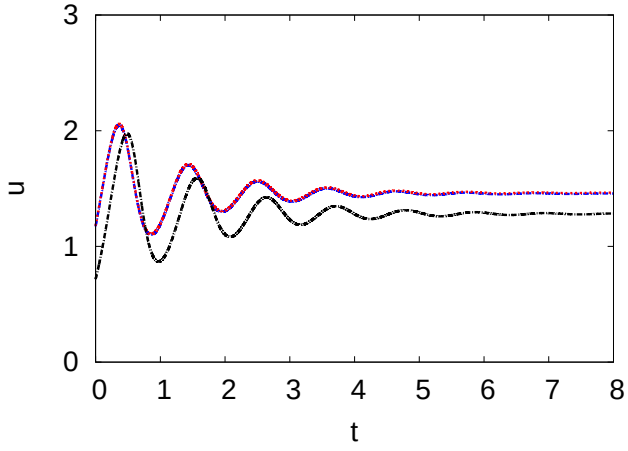

(c)

Figure 10: The evolution of u versus t, for (a) $x = 0$, (b) $x = 0.33$ (c) $x = 0.66$, for the 1-D domain. The one-term semi-analytical solution (black, solid line), the two-term semi-analytical solution (blue, dashed lines) and the numerical solution (red, dotted lines) are shown. The parameters are $\alpha = 0.8$, $\beta = 0.4$, $\gamma_1 = 0.1$, $D_1 = D_2 = 0.1$, $\delta_1 = 0.2$, $\gamma_2 = 0.7$, $\delta_2 = 0.5$ and $\tau_1 = \tau_2 = 1$.

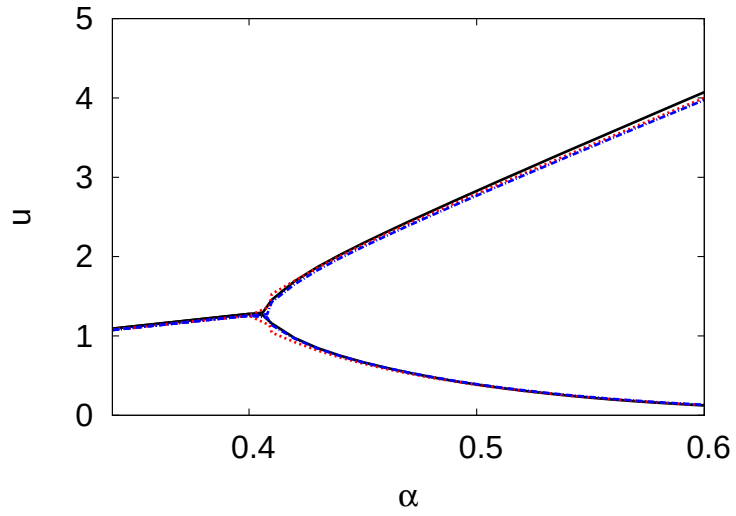

(a)

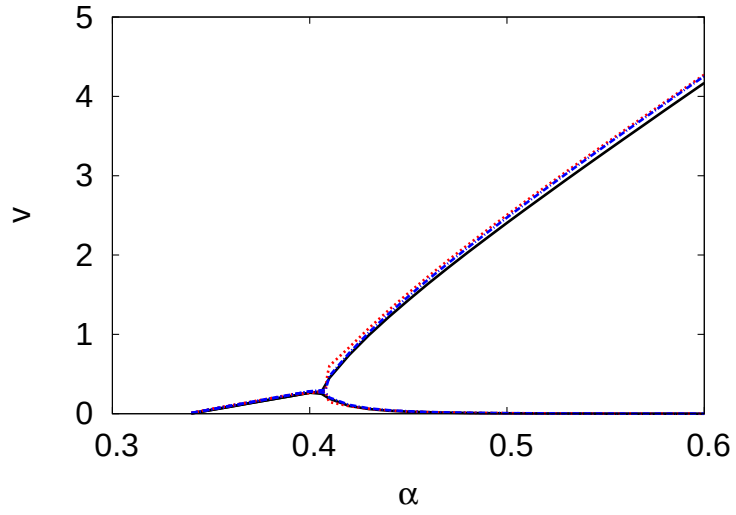

(b)

Figure 11: The bifurcation diagrams of u (a), and v (b), at $x = 0$, versus α for the 1-D spatial domain. The one-term semi-analytical solution (black solid line), the two-term semi-analytical solution (blue dashed line) and the numerical solution (red dotted line) are shown. The parameters are $\beta = 0.4$, $\gamma_1 = 0.1$, $D_1 = D_2 = 0.1$, $\delta_1 = 0.2$, $\gamma_2 = 0.7$, $\delta_2 = 0.5$ and $\tau_1 = \tau_2 = 4$.

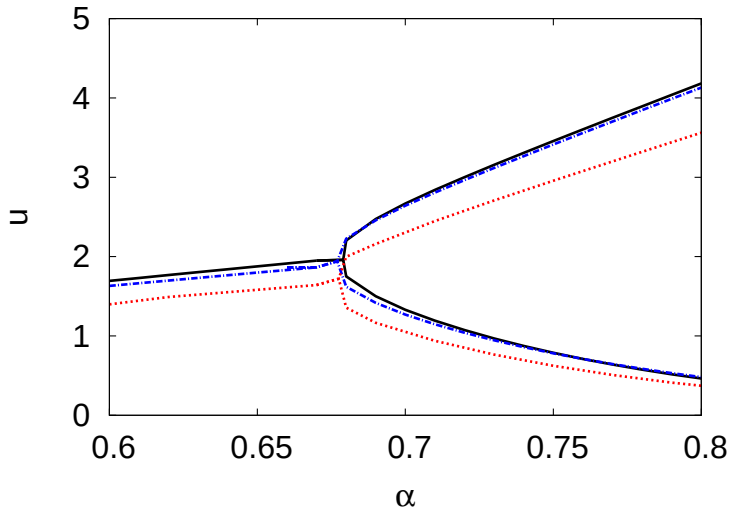

(a)

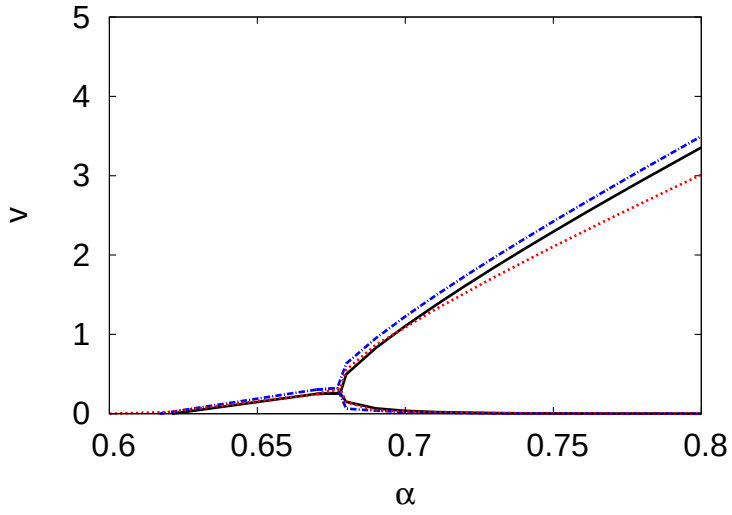

(b)

Figure 12: The bifurcation diagrams of u, (a), and v, (b), at $x = 0$, versus α for the 2-D spatial domain. The one-term semi-analytical solution (black solid line), the two-term semi-analytical solution (blue dashed line) and the numerical solution (red dotted line) are shown. The parameters are $\beta = 0.4$, $\gamma_1 = 0.1$, $D_1 = D_2 = 0.1$, $\delta_1 = 0.2$, $\gamma_2 = 0.7$, $\delta_2 = 0.5$ and $\tau_1 = \tau_2 = 4$.

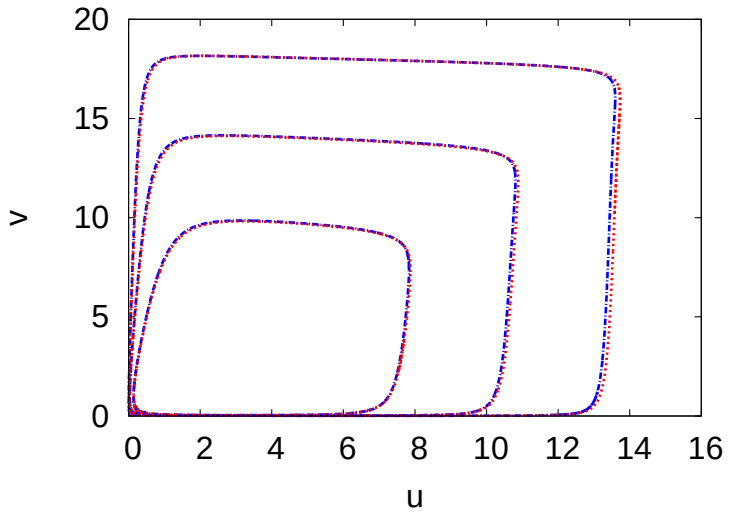

Figure 13: The limit cycle curve u versus v at $x = 0$ for $\alpha = 1$ (inner curves), $\alpha = 1.25$ (middle curves) and $\alpha = 1.5$ (outer curves), for the 1-D domain. Shown is the two-term semi-analytical solution (blue, dashed lines) and the numerical solution (red, dotted lines). The parameters are $\beta = 0.4$, $\gamma_1 = 0.1$, $D_1 = D_2 = 0.1$, $\delta_1 = 0.2$, $\gamma_2 = 0.7$, $\delta_2 = 0.5$ and $\tau_1 = \tau_2 = 2$.

period doubling and chaotic solutions. This behaviour does not occur for the classical two species Lokta-Volterra ode system without delay, as a minimum of three species is required for chaotic solutions, see Kozlov and Vakulenko [13]. An extensive numerical search of the parameter space for the diffusive delayed Loktka-Volerra system in 1-D and 2-D domains, (1) and (2), only yielded limit cycle solutions, beyond the relevant Hopf point, with no chaotic behaviour found. This figure shows that the amplitude of the oscillations continues to increase as α increases and that the limit cycle curve takes a near rectangular shape. The amplitudes of the oscillations are, for $\alpha = 1$, $(u, v) = (7.70, 9.87)$ (two-term) and $(u, v) = (7.79, 9.77)$ (numerical), for $\alpha = 1.25$, $(u, v) = (10.8, 14.1)$ (two-term) and $(u, v) = (10.9, 14.1)$ (numerical) and for $\alpha = 1.5$, $(u, v) = (13.6, 18.1)$ (two-term) and $(u, v) = (13.7, 18.2)$ (numerical). The two-term solution is extremely accurate, even for large α, with errors less than 1%.

5 Periodic solutions near the Hopf bifurcation point

An asymptotic analysis of the periodic solution of the semi-analytical DDEs model for the delayed Lotka-Volterra PDEs system (1) and (2) is developed for the 1-D domain. The Hopf perturbation technique, also called the Lindstedt-Poincaré method, is used to construct asymptotic limit cycle solutions of both the one- and two-term semi-analytical DDE models [6]. The power series method assumes that the oscillation amplitude ϵ is small and determines corrections to the frequency and bifurcation parameters by eliminating secular terms that appear in the expansion, at higher-order [14].

5.1 One-term solution

The one-term semi-analytical system is given by following DDEs

$$\begin{aligned}\frac{du_1}{dt} &= -\frac{\pi^2 D_1 u_1}{4} - \frac{8\gamma_1 u_1^2}{3\pi} - \frac{8\delta_1 u_1 v_{1d}}{3\pi} + \alpha u_1, \\ \frac{dv_1}{dt} &= -\frac{\pi^2 D_2 v_1}{4} - \frac{8\delta_2 v_1^2}{3\pi} - \beta v_1 + \frac{8\gamma_2 v_1 u_{1d}}{3\pi}.\end{aligned} \tag{9}$$

We assume a 2π-periodic solution of (9), of the form,

$$\begin{aligned}u_1(s) &= m_s + \epsilon m_1(s) + \epsilon^2 m_2(s) + \epsilon^3 m_3(s) + ..., \\ v_1(s) &= \eta_s + \epsilon \eta_1(s) + \epsilon^2 \eta_2(s) + \epsilon^3 \eta_3(s) + ...,\end{aligned} \tag{10}$$

where $s = \omega t$ is the scaled time variable and the parameter ϵ is the amplitude of the oscillation. This can be determined by a normalization condition as

$$\begin{aligned}&\epsilon = \frac{1}{2\pi}\int_0^{2\pi} m(s,\epsilon)\mathrm{e}^{-is}\,\mathrm{d}s,\ \frac{1}{2\pi}\int_0^{2\pi} m_1(s)\mathrm{e}^{-is}\,\mathrm{d}s = 1, \\ &\frac{1}{2\pi}\int_0^{2\pi} m_i(s)\mathrm{e}^{-is}\,\mathrm{d}s = 0,\ \forall i \neq 1.\end{aligned} \tag{11}$$

We expand both the bifurcation parameter α and the frequency ω by using a power series

$$\alpha = \alpha_0 + \epsilon^2 \alpha_2 + ...,\ \omega = \omega_0 + \epsilon^2 \omega_2 + ..., \tag{12}$$

where α_0 and ω_0 are the values of the parameters at the Hopf bifurcation point. The corrections α_2 and ω_2 are obtained by using solvability conditions at the third order of the perturbation analysis. Substituting equations (10) and (12) into (9), we obtain governing equations at the first three orders of ϵ, which are

$$\begin{aligned}&O(\epsilon):\ \omega_0 \acute{m_1} = \alpha_0 m_1 - \frac{16\gamma_1 m_s m_1}{3\pi} - \frac{8\delta_1 \eta_s m_1}{3\pi} - \frac{8\delta_1 m_s \eta_{1d}}{3\pi} - \frac{1}{4} D_1 \pi^2 m_1, \\ &\omega_0 \acute{\eta_1} = -\frac{16\delta_2 \eta_s \eta_1}{3\pi} - \frac{8\gamma_2 m_s \eta_1}{3\pi} + \frac{8\gamma_2 \eta_s m_{1d}}{3\pi} - \frac{1}{4} D_2 \pi^2 \eta_1 - \beta \eta_1,\end{aligned} \tag{13}$$

$$\begin{aligned}&O(\epsilon^2):\ \omega_0 \acute{m_2} = \alpha_0 m_2 - \frac{16\gamma_1 m_s m_2}{3\pi} - \frac{8\delta_1 \eta_s m_2}{3\pi} - \frac{8\delta_1 m_s \eta_{2d}}{3\pi} - \frac{1}{4} D_1 \pi^2 \eta_2 \\ &- \frac{8\delta_1 m_1 \eta_{1d}}{3\pi} - \frac{8\gamma_1 m_1^2}{3\pi}, \\ &\omega_0 \acute{\eta_2} = \frac{8\gamma_2 m_s \eta_2}{3\pi} - \frac{16\delta_2 \eta_s \eta_2}{3\pi} + \frac{8\gamma_2 \eta_s m_{2d}}{3\pi} - \frac{1}{4} D_2 \pi^2 \eta_2 - \beta \eta_2 \\ &+ \frac{8\gamma_2 \eta_1 m_{1d}}{3\pi} - \frac{8\delta_2 \eta_1^2}{3\pi},\end{aligned} \tag{14}$$

$$\begin{aligned}&O(\epsilon^3):\ \omega_0 \acute{m_3} = \frac{8\gamma_1 m_s \omega_2 \acute{\eta_{1d}}}{3\pi} - \frac{16\gamma_1 m_s m_3}{3\pi} - \frac{8\delta_1 \eta_s m_3}{3\pi} - \frac{8\delta_1 m_s \eta_{3d}}{3\pi} \\ &- \frac{1}{4} D_1 \pi^2 m_3 + \alpha_0 m_3 - \omega_2 \acute{m_1} - \frac{8\delta_1 m_1 \eta_{2d}}{3\pi} + \alpha_2 m_1 - \frac{16\gamma_1 m_1 m_2}{3\pi} - \frac{8\delta_1 m_2 \eta_{1d}}{3\pi}, \\ &\omega_0 \acute{\eta_3} = \frac{8\gamma_2 m_s \eta_3}{3\pi} - \frac{16\delta_2 \eta_s \eta_3}{3\pi} - \frac{16\delta_2 \eta_1 \eta_2}{3\pi} + \frac{8\gamma_2 \eta_s m_{3d}}{3\pi} - \frac{1}{4} D_2 \pi^2 \eta_3 \\ &- \beta \eta_3 - \frac{8\delta_2 \eta_s \omega_2 \acute{m_{1d}}}{3\pi} - \omega_2 \acute{\eta_1} + \frac{8\delta_2 \eta_1 m_{2d}}{3\pi} + \frac{8\delta_2 \eta_2 m_{1d}}{3\pi}.\end{aligned} \tag{15}$$

At the first two orders the solution of (13) and (14) are

$$\begin{aligned}&m_1(s) = \mathrm{e}^{is} + c.c.,\ \eta_1(s) = A\mathrm{e}^{is} + c.c., \\ &m_2(s) = B_1 \mathrm{e}^{2is} + c.c.,\ \eta_2(s) = B_2 \mathrm{e}^{2is} + c.c.,\end{aligned} \tag{16}$$

where *c.c.* is the complex conjugate. To find the amplitudes A, B_1 and B_2 of the oscillations in (16) we substitute (16) into (13) and (14) and separate into real and imaginary parts, see

(25) in the Appendix. At third-order we substitute the solutions (16) into (15) and obtain

$$\omega_0 \acute{m_3} + \frac{16\gamma_1 m_s m_3}{3\pi} + \frac{8\delta_1 \eta_s m_3}{3\pi} + \frac{8\delta_1 m_s \eta_{3d}}{3\pi} + \frac{1}{4} D_1 \pi^2 m_3 - \alpha_0 m_3 = \tag{17}$$
$$\mathrm{e}^{is}(\alpha_2 + \frac{8i\delta_1 m_s \omega_2 A \mathrm{e}^{-i\omega_0}}{3\pi} - i\omega_2 - \frac{16\gamma_1 B_1}{3\pi} - \frac{8\delta_1 B_2 \mathrm{e}^{-2i\omega_0}}{3\pi} - \frac{8\delta_1 B_1 A \mathrm{e}^{i\omega_0}}{3\pi}) + c.c.,$$
$$\omega_0 \acute{\eta_3} + \frac{16\delta_2 \eta_s \eta_3}{3\pi} - \frac{8\gamma_2 m_s \eta_3}{3\pi} - \frac{8\gamma_2 \eta_s m_{3d}}{3\pi} + \frac{1}{4} D_2 \pi^2 \eta_3 + \beta \eta_3 =$$
$$\mathrm{e}^{is}(\frac{8i\gamma_2 A B_1 \mathrm{e}^{-2i\omega_0}}{3\pi} + \frac{8i\gamma_2 \eta_s \omega_2 \mathrm{e}^{-i\omega_0}}{3\pi} - i\omega_2 A - \frac{16\delta_2 B_2 A}{3\pi} - \frac{8\gamma_2 B_2 \mathrm{e}^{i\omega_0}}{3\pi}) + c.c.,$$

where only the secular $\mathrm{e}^{\pm is}$ terms are shown on the r.h.s. of (17). The homogeneous form of the equations have the solution $(m_3,\eta_3)=c\mathrm{e}^{\pm is}(1,A)^T$ which can not be used to eliminate secular terms at $O(\epsilon^3)$. However, a choice orthogonal to this, such as $(m_3,\eta_3)=c\mathrm{e}^{\pm is}(1,0)^T$ is not a solution to the homogeneous equations. Thus, an appropriate choice of c together with α_2 and ω_2 eliminates the secular terms at $O(\epsilon^3)$, see (26) in the Appendix.

The solution is now complete and we explain the special case $\tau_1 = \tau_2 = 4$ in detail. The solution is given by

$$\begin{aligned} &(\alpha_0, \omega_0, m_s, \eta_s) = (0.410, 0.161, 1.310, 0.305), \\ &A = 0.033 - 0.879i,\ B_1 = -0.158 - 0.462i, \\ &B_2 = -1.130 - 0.279i,\ \alpha_2 = 0.133,\ \omega_2 = -0.371. \end{aligned} \tag{18}$$

The leading-order limit cycle and its period is given by

$$\begin{aligned} &u_1(s) \simeq m_s + \epsilon\cos(\omega t),\ v_1(s) \simeq \eta_s + \epsilon\Re(A\mathrm{e}^{is} + \bar{A}\mathrm{e}^{-is}), \\ &\epsilon \simeq \sqrt{7.51\alpha - 3.08},\ \omega \simeq 1.30 - 2.79\alpha, \end{aligned} \tag{19}$$

where the extrema of the oscillatory solutions are $u = m_s \pm 2\epsilon$ and $v = \eta_s \pm 1.76\epsilon$. The limit cycle (19) shows the classical square root behaviour near the Hopf point $\alpha = 0.410$. Also the frequency decreases linearly with α.

5.2 Two-term solution

The two-term semi-analytical equations are found from (4). The procedure for obtaining periodic solutions near the Hopf bifurcation point is similar to the one-term case. We assume a solution of (4) of the form

$$\begin{aligned} u_1(s) &= m_{s1} + \epsilon m_1(s) + \epsilon^2 m_2(s) + \epsilon^3 m_3(s), \\ v_1(s) &= \eta_{s1} + \epsilon \eta_1(s) + \epsilon^2 \eta_2(s) + \epsilon^3 \eta_3(s), \\ u_2(s) &= \xi_s + \epsilon \xi_1(s) + \epsilon^2 \xi_2(s) + \epsilon^3 \xi_3(s), \\ v_2(s) &= \rho_s + \epsilon \rho_1(s) + \epsilon^2 \rho_2(s) + \epsilon^3 \rho_3(s). \end{aligned} \tag{20}$$

The governing equations at the first three orders of ϵ are obtained by substituting (20) and (12) into (4). These perturbation equations are excessively long so are not presented here. Note that there are four equations at each order of ϵ. The first order solution has the form

$$\begin{aligned} &m_1(s) = \mathrm{e}^{is} + c.c.,\ \eta_1(s) = A_1\mathrm{e}^{is} + c.c., \\ &\xi_1(s) = A_2\mathrm{e}^{is} + c.c.,\ \ \rho_1(s) = A_3\mathrm{e}^{is} + c.c.. \end{aligned} \tag{21}$$

By substituting (21) into the $O(\epsilon)$ equations, three complex equations are obtained for the complex amplitudes A_1, A_2 and A_3. At $O(\epsilon^2)$, the solution has the following form

$$\begin{aligned} &m_2(s) = B_1\mathrm{e}^{2is} + c.c.,\ \eta_2(s) = B_2\mathrm{e}^{2is} + c.c., \\ &\xi_2(s) = B_3\mathrm{e}^{2is} + c.c.,\ \ \rho_2(s) = B_4\mathrm{e}^{2is} + c.c.. \end{aligned} \tag{22}$$

Again, by substituting (21) and (22) into the $O(\epsilon^2)$ equations, four complex equations are obtained for complex amplitudes B_1, B_2, B_3 and B_4. At the third order, the equations have

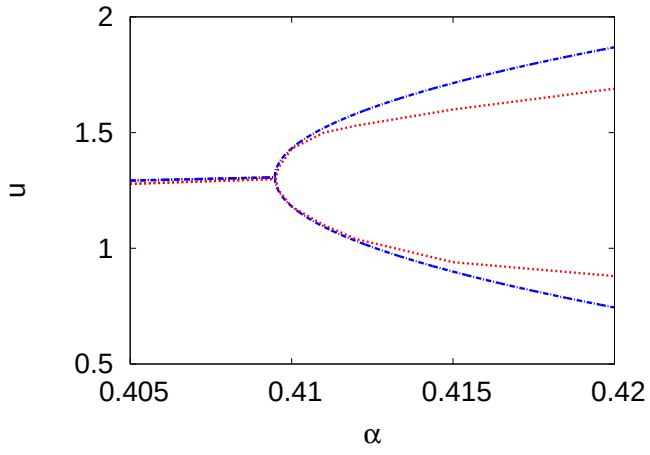

(a)

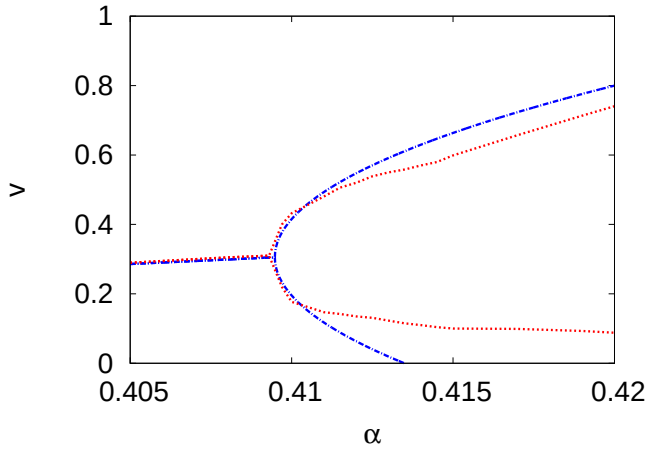

(b)

Figure 14: The bifurcation diagrams of u, (a), and v, (b), versus α. The one-term semi-analytical solution (red dotted lines) and the perturbation solution (blue dashed lines) are shown, for the 1-D domain The parameters are $\beta = 0.4$, $\gamma_1 = 0.1$, $D_1 = D_2 = 0.1$, $\delta_1 = 0.2$, $\gamma_2 = 0.7$, $\delta_2 = 0.5$ and $\tau_1 = \tau_2 = 4$.

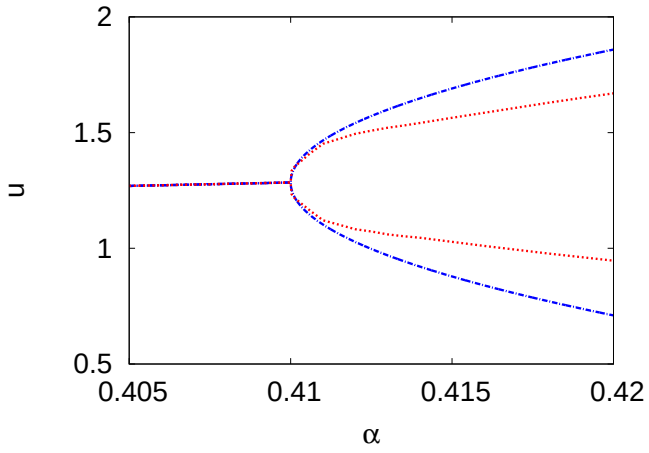

(a)

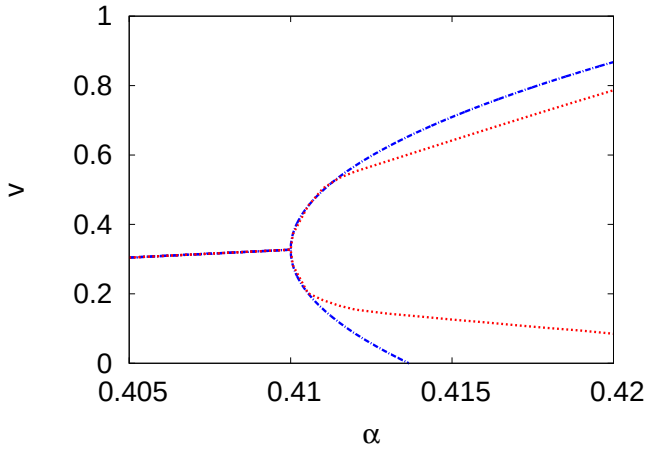

(b)

Figure 15: The bifurcation diagrams of u, (a), and v, (b), versus α. The two-term semi-analytical solution (red dotted lines) and the perturbation solution (blue dashed lines) are shown, for the 1-D domain. The parameters are $\beta = 0.4$, $\gamma_1 = 0.1$, $D_1 = D_2 = 0.1$, $\delta_1 = 0.2$, $\gamma_2 = 0.7$, $\delta_2 = 0.5$ and $\tau_1 = \tau_2 = 4$.

$e^{\pm is}$ terms on the r.h.s, which are secular terms. We let $(m_3, \eta_3, \xi_3, \rho_3) = c_1 e^{\pm is}(1,1,1,0)^T$ and choose c_1, α_2 and ω_0 to eliminate the secular terms at $O(\epsilon^3)$.

We illustrate the special case $\tau_1 = \tau_2 = 4$. The Hopf bifurcation solution is

$$\begin{aligned}
&(\alpha_0, \omega_0, m_{s1}, \eta_{s1}, \xi_s, \rho_s) = (0.410, 0.162, 1.310, 0.311, -0.023, 0.017), \\
&A_1 = 0.047 - 0.882i,\ A_2 = -0.014 + 0.198i,\ A_3 = 0.015 - 0.044i, \\
&B_1 = -0.131 - 0.462i,\ B_2 = -1.112 - 0.323i,\ B_3 = 0.021 + .0.003i, \\
&B_4 = -0.042 - 0.048i,\quad \alpha_2 = 0.118,\ \omega_2 = -0.366.
\end{aligned} \tag{23}$$

The leading-order limit cycle solution is

$$\begin{aligned}
&u(s) \simeq m_{s1} + \xi_s + \epsilon(2\cos(\omega t) + \Re\{A_2 e^{is} + \bar{A}_2 e^{-is}\}), \\
&v(s) \simeq \eta_{s1} + \rho_s + \epsilon(\Re\{A_1 e^{is} + \bar{A}_1 e^{-is} + A_3 e^{is} + \bar{A}_3 e^{-is}\}), \\
&\epsilon \simeq \sqrt{8.48\alpha - 3.48},\ \omega \simeq 1.43 - 3.10\alpha,
\end{aligned} \tag{24}$$

where the extrema of the oscillatory solutions are $u = 1.28 \pm 1.98\epsilon$ and $v = 0.327 \pm 1.857\epsilon$.

Figures 14 show the bifurcation diagram for u and v, for the one-term solution while figure 15 shows the two-term solution, both for the 1-D domain. Shown are semi analytical and perturbation solutions. The parameters are $\beta = 0.4$, $\gamma_1 = 0.1$, $D_1 = D_2 = 0.1$, $\delta_1 = 0.2$, $\gamma_2 = 0.7$, $\delta_2 = 0.5$ and $\tau_1 = \tau_2 = 4$. The solution loses stability at the Hopf point, $\alpha = 0.410$ for both the one- and two-term cases. The branches of oscillatory solutions form a near right angle with the steady state solution branch.These angles deviate slightly from the theoretically expected right angle due to the plotting of a finite number of points in the figures. Both figures show a good comparison between perturbation solutions and semi-analytical results for the interval $\alpha = [0.410, 0.413]$. The range of validity is limited by the fast growth of oscillatory amplitude, with respect to increasing α, and the limited range of accuracy for the Taylor-series expansion.

6 Conclusion

Semi-analytical DDE models have been developed for the diffusive Lotka-Volterra predator-prey system with delay in the 1-D and 2-D spatial domains. The DDE models are obtained as approximations to the governing PDEs. Bifurcation diagrams and Hopf bifurcation points are obtained for both the 1-D and 2-D domains and an asymptotic limit cycle solution developed, for the 1-D spatial domain. The method used here has proved to be highly effective in generating accurate approximate solutions and is applicable to a wide range of reaction-diffusion equations, both with and without delay terms.

A Equations associated with the one-term periodic solution

The transcendental equations for the amplitudes $A = A_r + iA_i$, $B_1 = B_{1r} + iB_{1i}$ and $B_2 = B_{2r} + iB_{2i}$ are

$$\begin{aligned}
&\alpha_0 - \frac{16}{3\pi}\gamma_1 m_s - \frac{8}{3\pi}\delta_1\eta_s - \frac{8}{3\pi}\delta_1 m_s A_r \cos(\omega_0\tau_1) - \frac{8}{3\pi}\delta_1 m_s A_i \sin(\omega_0\tau_1) - \frac{1}{4}D_1\pi^2 = 0, \\
&\omega_0 - \frac{8}{3\pi}\delta_1 m_s A_r \sin(\omega_0\tau_1) + \frac{8}{3\pi}\delta_1 m_s A_i \cos(\omega_0\tau_1) = 0, \\
&\omega_0 A_i - \frac{16}{3\pi}\delta_2\eta_s A_r + \frac{8}{3\pi}\gamma_2 m_s A_r + \frac{8}{3\pi}\gamma_2\eta_s \cos(\omega_0\tau_2) - \frac{1}{4}D_2\pi^2 A_r - \beta A_r = 0, \\
&\omega_0 A_r + \frac{16}{3\pi}\delta_2\eta_s A_i - \frac{8}{3\pi}\gamma_2 m_s A_i + \frac{8}{3\pi}\gamma_2\eta_s \sin(\omega_0\tau_2) + \frac{1}{4}D_2\pi^2 A_i + \beta A_i = 0, \\
&2\omega_0 B_{1i} - \frac{16}{3\pi}\gamma_1 m_s B_{1r} - \frac{8}{3\pi}\delta_1\eta_s B_{1r} - \frac{8}{3\pi}\delta_1 m_s B_{2r}\cos(2\omega_0\tau_1) - \frac{8}{3\pi}\gamma_1
\end{aligned} \tag{25}$$

$$
\begin{aligned}
&-\frac{8}{3\pi}\delta_1 A_r\cos(\omega_0\tau_1)-\frac{8}{3\pi}\delta_1 m_s B_{2i}\sin(2\omega_0\tau_1)-\frac{8}{3\pi}\delta_1 A_i\sin(\omega_0\tau_1)\\
&+\alpha_0 B_{1r}-\frac{1}{4}D_1\pi^2 B_{1r}=0,\\
&\alpha_0 B_{1i}-2\omega_0 B_{1r}-\frac{16}{3\pi}\gamma_1 m_s B_{1i}-\frac{8}{3\pi}\delta_1\eta_s B_{1i}-\frac{8}{3\pi}\delta_1 m_s B_{2i}\cos(2\omega_0)\\
&-\frac{1}{4}D_1\pi^2 B_{1i}+\frac{8}{3\pi}\delta_1 A_r\sin(\omega_0\tau_1)-\frac{8}{3\pi}\delta_1 A_i\cos(\omega\tau_1)+\frac{8}{3\pi}\delta_1 m_s B_{2r}\sin(2\omega_0\tau_1)=0,\\
&2i\omega_0 B_{2i}+\frac{8}{3\pi}\gamma_2 A_r\cos(\omega_0\tau_2)+\frac{8}{3\pi}\gamma_2 A_i\sin(\omega_0\tau_2)-\frac{8}{3\pi}\gamma_2\eta_s B_{1i}\sin(2\omega_0\tau_2)-\frac{16}{3\pi}\delta_2\eta_s B_{2r}\\
&+\frac{8}{3\pi}\gamma_2 m_s B_{2r}-\frac{8}{3\pi}\gamma_2\eta_s B_{1r}\cos(2\omega_0\tau_2)-\beta B_{2r}-\frac{8}{3\pi}\delta_2 A_r^2-\frac{1}{4}D_2\pi^2 B_{2r}=0,\\
&-2\omega_0 B_{2r}-\frac{8}{3\pi}\gamma_2 A_r\sin(\omega_0\tau_2)+\frac{8}{3\pi}\gamma_2 A_i\cos(\omega_0\tau_2)+\frac{8}{3\pi}\gamma_2\eta_s B_{1r}\sin(2\omega_0\tau_2)-\frac{16}{3\pi}\delta_2\eta_s B_{2i}\\
&+\frac{8}{3\pi}\gamma_2 m_s B_{2i}-\frac{16}{3\pi}\delta_2 A_i A_r-\frac{1}{4}D_2\pi^2 B_{2i}-\beta B_{2i}-\frac{8}{3\pi}\gamma_2\eta_s B_{1i}\cos(2\omega_0\tau_2)=0.
\end{aligned}
$$

The transcendental equations for $c=c_r+ic_i$, α_2 and ω_2 are

$$
\begin{aligned}
&\omega_0 c_i-\frac{16}{3\pi}\delta_1\sin(\omega_0\tau_1)\cos(\omega_0\tau_1)B_{2i}-\frac{8}{3\pi}\delta_1 m_{ss}c_r-\frac{1}{4}\pi^2 D_1\,c_r-\frac{8}{3\pi}\delta_1 B_{1r}A_{2r}\cos(\omega_0\tau_1)\\
&-\frac{8}{3\pi}\delta_1 B_{1r}A_{2i}\sin(\omega_0\tau_1)+\alpha_0 c_r+\frac{8}{3\pi}\delta_1 B_{1i}A_{2r}\sin(\omega_0\tau_1)-\frac{8}{3\pi}\delta_1 B_{1i}A_{2i}\cos(\omega_0\tau_1)\\
&-\frac{16}{3\pi}\gamma_1 B_{2r}-\frac{16}{3\pi}\delta_1\cos(\omega_0\tau_1)^2 B_{2r}+\frac{8}{3\pi}\delta_1 m_s\omega_2\sin(\omega_0\tau_1)A_{2r}+\alpha_2-\frac{16}{3\pi}\gamma_1 m_s c_r\\
&-\frac{8}{3\pi}\delta_1 m_s\omega_2\cos(\omega_0\tau_1)A_{2i}+\frac{8}{3\pi}\delta_1 B_{2r}=0,\\
&-\omega_0 c_r-\frac{16}{3\pi}\gamma_1 m_s c_i-\frac{8}{3\pi}\delta_1 m_{ss}c_i-\frac{16}{3\pi}\delta_1\cos(\omega_0\tau_1)^2 B_{2i}-\frac{1}{4}\pi^2 D_1 c_i-\frac{16}{3\pi}\gamma_1 B_{1i}\\
&+\frac{8}{3\pi}\delta_1 m_s\omega_2\cos(\omega_0\tau_1)A_{2r}+\frac{8}{3\pi}\delta_1 m_s\omega_2\sin(\omega_0\tau_1)A_{2i}-\frac{8}{3\pi}\delta_1 B_{1i}A_{2r}\cos(\omega_0\tau_1)\\
&-\frac{8}{3\pi}\delta_1 B_{1r}A_{2r}\sin(\omega_0\tau_1)+\alpha_0 c_i-\omega_2+\frac{16}{3\pi}\delta_1\sin(\omega_0\tau_1)\cos(\omega_0\tau_1)B_{2r}\\
&-\frac{8}{3\pi}\delta_1 B_{1i}A_{2i}\sin(\omega_0\tau_1)+\frac{8}{3\pi}\delta_1 B_{2i}+\frac{8}{3\pi}\delta_1 B_{1r}A_{2i}\cos(\omega_0\tau_1)=0,
\end{aligned}
\tag{26}
$$

$$
\begin{aligned}
&\omega_2 A_{2i}+\frac{8}{3\pi}\gamma_2 m_{ss}\cos(\omega_0\tau_2)c_r+\frac{8}{3\pi}\gamma_2 m_{ss}\sin(\omega_0\tau_2)c_i-\frac{16}{3\pi}\delta_2 A_{2i}B_{2i}+\frac{16}{3\pi}\gamma_2\cos(\omega_0\tau_2)^2 A_{2i}B_{1i}\\
&-\frac{8}{3\pi}\gamma_2 m_{ss}\omega_2\sin(\omega_0\tau_2)-\frac{8}{3\pi}\gamma_2 B_{1r}A_{2r}-\frac{16}{3\pi}\gamma_2\sin(\omega_0\tau_2)\cos(\omega_0\tau_2)A_{2i}B_{1r}-\frac{16}{3\pi}\delta_2 A_{2r}B_{2r}\\
&-\frac{8}{3\pi}\gamma_2 B_{1i}A_{2i}+\frac{16}{3\pi}\gamma_2\sin(\omega_0\tau_2)\cos(\omega_0\tau_2)A_{2r}B_{1i}+\frac{8}{3\pi}\gamma_2 B_{2r}\cos(\omega_0\tau_2)+\frac{16}{3\pi}\gamma_2\cos(\omega_0\tau_2)^2 A_{2r}B_{1r}\\
&-\frac{8}{3\pi}\gamma_2 B_{2i}\sin(\omega_0\tau_2)=0,\\
&-\omega_2 A_{2r}-\frac{16}{3\pi}\gamma_2\sin(\omega_0\tau_2)\cos(\omega_0\tau_2)A_{2r}B_{1r}+\frac{16}{3\pi}\gamma_2\cos(\omega_0\tau_2)^2 A_{2r}B_{1i}+\frac{8}{3\pi}\gamma_2 B_{2r}\sin(\omega_0\tau_2)\\
&+\frac{8}{3\pi}\gamma_2 B_{2i}\cos(\omega_0\tau_2)-\frac{16}{3\pi}\delta_2 A_{2r}B_{2i}-\frac{8}{3\pi}\gamma_2 B_{1i}A_{2r}-\frac{8}{3\pi}\gamma_2 m_{ss}\omega_2\cos(\omega_0\tau_2)\\
&+\frac{8}{3\pi}\gamma_2 m_{ss}\cos(\omega_0\tau_2)c_i-\frac{8}{3\pi}\gamma_2 m_{ss}\sin(\omega_0\tau_2)c_r-\frac{16}{3\pi}\gamma_2\sin(\omega_0\tau_2)\cos(\omega_0\tau_2)A_{2i}B_{1i}\\
&-\frac{16}{3\pi}\gamma_2\cos(\omega_0\tau_2)^2 A_{2i}B_{1r}+\frac{16}{3\pi}\delta_2 A_{2i}B_{2r}+\frac{8}{3\pi}\gamma_2 A_{2i}B_{1r}=0.
\end{aligned}
$$

Acknowledgements

K.S. Al Noufaey gratefully thanks Taif University in Saudi Arabia for awarding him a PhD scholarship to study at the University of Wollongong, Australia. The authors would also like to thank the two anonymous referees for their helpful comments.

References

[1] H. Y. Alfifi, T. R. Marchant and M. I. Nelson, Semi-analytical solutions for the 1- and 2-D diffusive Nicholsons blowflies equation, *IMA J. Appl. Math.* **79** (2014) 175-199.

[2] H. Y. Alfifi, T. R. Marchant and M. I. Nelson, Generalised diffusive delay logistic equations: semi-analytical solutions, *Dyn. Contin. Discrete Ser. B.* **19** (2012) 579–596.

[3] K. S. Al Noufaey and T. R. Marchant, Semi-analytical solutions for the reversible Selkov model with feedback delay, *Appl. Math. Comput.* **232** (2014) 49–59.

[4] S. Busenberg and W. Huang, Stability and Hopf bifurcation for a population delay model with diffusion effects, *Diff. Eqs.* **124** (1996) 80–127.

[5] S.S. Chen, J.P. Shi and J.J. Wei, A note on Hopf bifurcations in a delayed diffusive Lotka-Volterra predator-prey system, *Comput. Math. Appl.* **62** (2011) 2240–2245.

[6] T. Erneux, Applied Delay Differential Equations, *Springer, New York* (2009).

[7] W.F. Fagan, R.S. Cantrell and C. Cosner, How habitat edges change species interactions, *Amer. Nat.* **153** (1999) 165-182.

[8] T. Faria, Stability and bifurcation for a delayed predator-prey model and the effect of diffusion, *Math. Anal. Appl.* **254** (2001) 433–463.

[9] T. Faria, Bifurcation aspects from some delayed population models with diffusion, *Fields Inst. Commun.* **21** (1999) 143–158.

[10] G. Galiano, M.L. Garzón and A. Jüngel, Analysis and numerical solution of a nonlinear cross-diffusion system arising in population dynamics, *Rev. Real Acad. Ciencias, Serie A. Mat.* **95** (2001) 281–295.

[11] A. S. Hacinliyan, I. Kusbeyzi and O. O. Aybar, Approximate solutions of Maxwell Bloch equations and possible Lotka-Volterra type behavior, *Nonlinear Dynamics* **62** (2010) 17–26.

[12] J. Hale, Theory of Functional Differential Equations, *Springer Verlag, New York*, (1977).

[13] V. Kozlov and S. Vakulenko, On chaos in Lokta-Volterra systems: an analytical approach, *Nonlinearity* **26** (2013) 2299-2314.

[14] G. looss and D. D. Joseph, Elementary Stability and Bifurcation Theory, *New York:Springer*, (1990).

[15] A. Lotka, Elements Of Physical Biology, *Williams & Wilkins Company, Baltimore* (1925).

[16] T. R. Marchant, Cubic autocatalytic reaction-diffusion equations: semi-analytical solutions, *Proc. Roy. Soc. Lond A* **458** (2002) 873-888.

[17] T. R. Marchant, Cubic autocatalysis with Michaelis-Menten kinetics: semi-analytical solutions for the reaction-diffusion cell, *Chem. Engng. Sci.* **59** (2004) 3433–3440.

[18] K. Miroslav, Delay Compensation for Nonlinear, Adaptive, and PDE Systems, *Birkhauser Boston Inc*, (2009).

[19] M.I. Nelson, T. R. Marchant, G.C. Wakeb, E. Balakrishnan and X.D. Chen, Self-heating in compost piles due to biological effects, *Chem. Engng. Sci.* **62** (2007) 4612-4619.

[20] X. Shenghu, Dynamics of a general prey-predator model with prey-stage structure and diffusive effects, *Comput. Math. Appl.* **68** (2014) 405–423.

[21] Y. Wang, Asymptotic behavior of solutions for a class of predator-prey reaction-diffusion systems with time delays, *Math. Anal. Appl.* **328** (2007) 137–150.

[22] X.-P. Yan and Y.-D. Chu, Stability and bifurcation analysis for a delayed Lotka-Volterra predator-prey system, *Comput. Appl. Math.* **196** (2006) 198–210.

[23] X. Zhang and H. Zhao, Bifurcation and optimal harvetsing of a diffusive predator-prey system with delays and interval biological parameters, *J. Theor. Biol.* **363** (2014) 390-403.